Synthesis in Molten Alkali Metal Polyselenophosphate Fluxes: A New Family of Transition Metal Selenophosphate Compounds, $A_2MP_2Se_6$ (A = K, Rb, Cs; M = Mn, Fe) and $A_2M'_2P_2Se_6$ (A = K, Cs; M′ = Cu, Ag)

Timothy J. McCarthy and Mercouri G. Kanatzidis*,†

Department of Chemistry and the Center for Fundamental Materials Research, Michigan State University, East Lansing, Michigan 48824

Received August 18, 1994[⊗]

Five isostructural quaternary alkali metal transition metal selenophosphate compounds, $K_2MnP_2Se_6$ (**I**), $Rb_2MnP_2Se_6$ (**II**), $Cs_2MnP_2Se_6$ (**III**), $K_2FeP_2Se_6$ (**IV**), and $Cs_2FeP_2Se_6$ (**V**), were synthesized by the molten alkali polyselenophosphate flux technique. In addition, the compounds $Cs_2Cu_2P_2Se_6$ (**VI**), $K_2Ag_2P_2Se_6$ (**VII**), and $Cs_2Ag_2P_2Se_6$ (**VIII**) were synthesized similarly but possess different structures. Crystals were grown with $M/P_4Se_{10}/A_2Se/Se$ flux reactions at 450 °C while pure material was obtained by direct combination of $Mn/P/A_2Se/Se$ at 500 °C. The structures of **I**, **III**, **IV**, **VI**, **VII**, and **VIII** have been determined by single-crystal X-ray diffraction analysis. Orange crystals of **I** crystallize in the monoclinic space group $P2_1/n$ (No. 14) with $a = 6.5349(9)$ Å, $b = 12.696(3)$ Å, $c = 7.589(2)$ Å, $\beta = 102.67(2)°$, $V = 614.3(4)$ Å^3, and $Z = 2$. Compound **III** also crystallizes in the space group $P2_1/n$ (No. 14) with $a = 6.4761(9)$ Å, $b = 13.006(2)$ Å, $c = 7.974(1)$ Å, $\beta = 93.09(1)°$, $V = 670.6(2)$ Å^3, and $Z = 2$. Red crystals of **IV** are X-ray isomorphous to **I** with $a = 6.421(2)$ Å, $b = 12.720(5)$ Å, $c = 7.535(3)$ Å, $\beta = 102.58(3)°$, $V = 600.7(7)$ Å^3, and $Z = 2$. Dark green crystals of **VI** are also monoclinic, space group $P2_1/c$ (No. 14), with $a = 9.958(3)$ Å, $b = 13.067(3)$ Å, $c = 10.730(2)$ Å, $\beta = 102.46(2)°$, $V = 1363(1)$ Å^3, and $Z = 4$. Orange crystals of **VII** are monoclinic, space group $P2_1/c$ (No. 14) with $a = 8.528$ Å, $b = 11.251(6)$ Å, $c = 20.975(4)$ Å, $\beta = 93.24(3)°$, $V = 2009(3)$ Å^3, and $Z = 4$. Yellow rod-like crystals of **VIII** crystallize in the monoclinic space group $P2_1/n$ (No. 14) with $a = 6.807(3)$ Å, $b = 12.517(3)$ Å, $c = 8.462(3)$ Å, $\beta = 95.75(3)°$, $V = 717.3(8)$ Å^3, and $Z = 2$. The structure of the $[MP_2Se_6]_n^{2n-}$ (M = Mn, Fe) anion (**I**−**V**) is closely related to the TiI_3 structure type. The transition metal ion and the P−P pairs reside in octahedra that share faces in the *a*-direction. These chains are well separated by alkali metal ions. The structures of **VI** and **VIII** are closely related to those of **I**−**V**. Cu···Cu and Ag···Ag dimers are found in the octahedral metal sites to form the chain structure. The structure of **VII** is unrelated to the chain structure but forms a three-dimensional tunnel framework consisting of tetrahedral $AgSe_4$ and $[P_2Se_6]^{4-}$ units. Magnetic susceptibility measurements indicate that **I**−**IV** couple antiferromagnetically between 10 and 20 K and the d electrons of M^{2+} are found in a high-spin state. The band gaps were determined by optical spectroscopy to be 2.33, 2.41, 2.19, 1.72, and 2.02 eV respectively for **I**−**V**. The band-gaps of **VI**−**VIII** can be assessed at 2.44, 2.39, and 2.55 eV respectively. All compounds melt congruently with **I** melting at 717 °C, **II** at 781 °C, **III** at 831 °C, **IV** at 662 °C, **V** at 769 °C, **VI** at 670 °C, **VII** at 542 °C, and **VIII** at 594 °C.

Introduction

Recently, we have developed the chalcophosphate flux method to synthesize several quaternary main group compounds, $ABiP_2S_7$ (A = K, Rb),[1] KMP_2Se_6 (M = Sb, Bi)[2] and $Cs_8M_4(P_2Se_6)_5$ (M = Sb, Bi).[3] The $A_x[P_yQ_z]$ (Q = S, Se) fluxes provide excess $A_x[P_yQ_z]^{n-}$ anions which bind the metal ions and perhaps also act as mineralizers. Using polyselenophosphate $A_x[P_ySe_z]$ fluxes below 600 °C, we wanted to explore the chemistry of first row transition metals to see if this strongly basic medium would discourage the formation of the well-known $M_2P_2Se_6$ compounds. The $M_2P_2Q_6$ (M = Mn, Fe, Co, Ni, Zn, Cd, V, Mg; Q = S, Se) family of compounds are structurally related to CdI_2.[4,5] These compounds possess interesting magnetic[6] and intercalation properties[7] and transition metal thiophosphates are of potential importance as low-dimensional cathode materials for secondary lithium batteries.[8] Substitution of M^{2+} cations by M^+ (Ag, Cu) and M^{3+} (Al, In, Cr, V) has been demonstrated for $M_2P_2Q_6$ compounds to form quaternary chalcophosphates which retain the stable CdI_2

† Camille and Henry Dreyfus Teacher-Scholar 1993−1995.

[⊗] Abstract published in *Advance ACS Abstracts,* February 1, 1995.

(1) McCarthy, T. J.; Kanatzidis, M. G. *Chem. Mater.* **1993**, *5*, 1061−1063.
(2) McCarthy, T. J.; Kanatzidis, M. G. *J. Chem. Soc., Chem. Commun.* **1994**, 1089−1090.
(3) McCarthy, T. J.; Hogan, T.; Kannewurf, C. R.; Kanatzidis, M. G. *Chem. Mater.* **1994**, *6*, 1072−1079.
(4) (a) Klingen, W.; Eulenberger, G.; Hahn, H. *Z. Anorg. Allg. Chem.* **1973**, *401*, 97−112. (b) Toffoli, P.; Khodadad, P.; Rodier, N. *Acta Cryst., Sect. B* **1978**, *34*, 1779−1781. (c) Klingen, W.; Ott, R.; Hahn, H. *Z. Anorg. Allg. Chem.* **1973**, *396*, 271−278. (d) Jandali, M. Z.; Eulenberger, G.; Hahn, H. *Z. Anorg. Allg. Chem.* **1978**, 447, 105−118.
(5) (a) Ouvrard, G.; Brec, R.; Rouxel, J. *Mater. Res. Bull.* **1985**, *20*, 1181−1189. (b) Lee, S.; Colombet, P.; Ouvrard, G.; Brec, R. *Inorg. Chem.* **1988**, *27*, 1291−1294. (c) Lee, S.; Colombet, P.; Ouvrard, G.; Brec, R. *Mater. Res. Bull.* **1986**, *21*, 917−928. (d) Durand, E.; Ouvrard, G.; Evain, M.; Brec, R. *Inorg. Chem.* **1990**, *29*, 4916−4920.
(6) (a) Odile, J.-P.; Steger, J. J.; Wold, A. *Inorg. Chem.* **1975**, *14*, 2400−2402. (b) Taylor, B. E.; Steger. J. J.; Wold, A.; Kostiner, E. *Inorg. Chem.* **1974**, *13*, 2719−2421. (c) Taylor, B. E.; Steger, J. J.; Wold, A. *J. Solid State Chem.* **1973**, *7*, 461−467.
(7) (a) Lagadic, I.; Leaustic, A.; Clement, R. *J. Chem. Soc., Chem. Commun.* **1992**, 1396−1397. (b) Clement, R.; Audiere, J.-P.; Renard, J.-P. *Rev. Chim. Miner.* **1982**, *19*, 560−571. (b) Michalowicz, A.; Clement R. *Inorg. Chem.* **1982**, *21*, 3872−3877. (c) Clement R. *J. Chem. Soc., Chem. Commun.* **1980**, 647−648. (d) Joy, P. A.; Vasudevan, S. *J. Am. Chem. Soc.* **1981**, *114*, 7792−7801.
(8) Thompson, A. H.; Whittingham, M. S. U.S. Patent 4,049,879 1977. (b) Brec, R.; Le Mehauté, A. Fr. Patents 7,704,519 1977.

0020-1669/95/1334-1257$09.00/0

structure-type.[9] Recently, Clement and co-workers have reported that ion-exchange intercalation of $M_2P_2S_6$ (M = Cd, Mn) with a cationic organic dye induces a large second-order optical nonlinearity and permanent magnetization (Mn^{2+}).[10]

Although $[P_xSe_y]^{n-}$ units such as $[PSe_4]^{3-}$ and $[P_2Se_6]^{4-}$ are interesting because of the many different bonding modes they can potentialy exhibit, relatively little is known about the coordination chemistry of these ligands. Presumably, progress in this area has been hindered by the lack of suitable solvents for the dissolution of these highly charged ligands. The rare $[PSe_4]^{3-}$ ligand is found in solid state compounds such as Cu_3PSe_4[11] and Tl_3PSe_4.[12] Kolis and co-workers have isolated two transition metal complexes with unusual coordinating $[PSe_2]^-$ and $[PSe_5]^{3-}$ ligands by using "P_4Se_4" glasses in DMF solutions.[13] We have shown recently that the use of molten alkali selenophosphate fluxes is a convenient method for stabilizing highly charged $[P_xSe_y]^{n-}$ units.[2,3]

Here we report the synthesis, structural characterization, and optical, thermal and magnetic properties of a new class of compounds, $A_2MP_2Se_6$ (A = K, Rb, Cs; M = Mn, Fe) and $A_2M'_2P_2Se_6$ (A = K, Cs; M' = Cu, Ag). In the case of Mn and Fe, successful dismantling of the $M_2P_2Se_6$ framework results in the formation of one-dimensional, polymeric anions that are reminiscent of the TiI_3 structure type. Replacement of the octahedral M^{2+} metal centers with $M'^{+}\cdots M'^{+}$ (M' = Cu, Ag) pairs gives rise to $Cs_2M'P_2Se_6$. In $A_2M'_2P_2Se_6$, a change in the counterion size (A) (substitution of Cs^+ with K^+) results in dramatic change in structure from a one-dimensional chain to a complex three-dimensional tunnel framework.

2. Experimental Section

2.1. Reagents. Chemicals in this work were used as obtained: (i) iron metal powder, 99.9% purity, −325 mesh, Cerac Inc., Milwaukee, WI; (ii) manganese metal powder, 99.9% purity −50 mesh, Aldrich Chemical Co., Inc., Milwaukee, WI; (iii) copper and silver metal powders, Fisher Scientific Co., Fair Lawn, NJ; (iv) red phosphorous powder, Morton Thiokol, Inc., −100 mesh, Danvers, MA; (v) selenium powder, 99.5+% purity −100 mesh, Aldrich Chemical Co., Inc., Milwaukee, WI; (vi) potassium metal, Aldrich Chemical Co., Inc., Milwaukee, WI; (vii) rubidium metal and cesium metal, analytical reagent, Johnson Matthey/AESAR Group, Seabrook, NH; (viii) DMF, analytical reagent, diethyl ether, ACS anhydrous, EM Science, Inc., Gibbstown, NJ; (ix) triethylphosphine, Aldrich Chemical Co., Inc., Milwaukee, WI.

2.2. Syntheses. All manipulations were carried out under a dry nitrogen atmosphere in a Vacuum Atmospheres Dri-Lab glovebox. For the preparation of K_2Se, Rb_2Se, and Cs_2Se we used a modified literature procedure.[14] The preparation of K_2Se has been reported elsewhere.[15]

Cs_2Se. A 5.00 g (0.038 mol) sample of slightly heated (~30°C) cesium metal was pipetted into a 250 mL round-bottom flask. A 150 mL volume of liquid ammonia was condensed into the flask at −78 °C (dry ice/acetone bath) under nitrogen to give a dark blue solution. Selenium (1.485 g, 0.019 mol) and a Teflon-coated stir bar were added, and the mixture was stirred for 1 h to give a light blue solution. The NH_3 was removed by evaporation under a flow of nitrogen as the bath slowly warmed to room temperature. The pale orange solid (98% yield) was dried under vacuum overnight, flame-dried, and ground to a fine powder in the glove box.

Rb_2Se. The same procedure as for Cs_2Se was used.

P_2Se_5. The amorphous phosphorus selenide glass, "P_2Se_5", was prepared by heating a stoichiometric ratio of the elements (red phosphorous was used) in an evacuated pyrex tube for 24 h at 460 °C. The glass was ground up and stored in a nitrogen glovebox.

$K_2MnP_2Se_6$ (I). A 0.014 g (0.25 mmol) sample of Mn, 0.228 g (0.50 mmol) of P_2Se_5, 0.079 g (0.50 mmol) of K_2Se, and 0.197 g (2.50 mmol) of Se were thoroughly mixed and transferred to a 6 mL pyrex tube which was subsequently flame-sealed in vacuo (~10^{-3} Torr). The reaction was heated to 450 °C over 12 h in a computer-controlled furnace. It was kept at 450 °C for 6 days, followed by cooling to 150 °C at a rate of 4 °C/h, and then to room temperature in 1 h. The moisture-sensitive product was isolated by dissolving the flux with degassed DMF under inert atmosphere and then washed with anhydrous ether to give orange needle-like crystals and a small amount of gray powder (crystallized flux). Semiquantitative microprobe analysis on single crystals gave $K_{2.2}Mn_{1.0}P_{2.5}Se_{6.5}$ (average of three data acquisitions). These crystals were used for crystallographic studies. Pure material was obtained by heating Mn/P/K_2Se/Se in a stoichiometric ratio in a pyrex tube at 500 °C for 4 days. The product was washed with degassed DMF and ether to give 0.378 g (56% yield, based on Mn) of orange crystallites. Far-IR (CsI matrix) shows absorptions at 478 (s), 463 (s), 303 (m), and 210−143 (w) cm^{-1}.[16]

$Rb_2MnP_2Se_6$ (II). Pure material was obtained by heating a stoichiometric ratio of Mn/P/Rb_2Se/Se as above to give 0.396 g (52% yield, based on Mn) of orange rod-like crystallites. The crystallites are moisture sensitive. Semiquantitative microprobe analysis on single crystals gave $Rb_{1.8}Mn_{1.0}P_{1.5}Se_{4.7}$ (average of three data acquisitions). Far-IR (CsI matrix) shows absorptions at 480 (s), 465 (s), 304 (m), and 201−148 (w) cm^{-1}.

$Cs_2MnP_2Se_6$ (III). A 0.014 g (0.25 mmol) sample of Mn, 0.228 g (0.50 mmol) of P_2Se_5, 0.157g (0.46 mmol) of Cs_2Se, and 0.197 g (2.50 mmol) of Se were heated as above. The product was isolated by dissolving the flux with degassed DMF under inert atmosphere and then washed with anhydrous ether to give orange needle-like crystals and elemental Se. The crystals appear to be stable in water. Semiquantitative microprobe analysis on single crystals gave $Cs_{2.0}Mn_{1.0}P_{2.2}Se_{6.3}$ (average of three data acquisitions). These crystals were used for crystallographic studies. Pure material was obtained by heating Mn/P/Cs_2Se/Se in a stoichiometric ratio as above to give 0.423 g (49% yield, based on Mn) of orange crystallites. Far-IR (CsI matrix) shows absorptions at 481 (s), 464 (s), 305 (m), and 189−152 (w) cm^{-1}.

$K_2FeP_2Se_6$ (IV). A 0.014 g (0.25 mmol) sample of Fe, 0.228 g (0.50 mmol) of P_2Se_5, 0.079 g (0.50 mmol) of K_2Se, and 0.197 g (2.50 mmol) of Se were heated as in the procedure used for **I** except for 4 days. The moisture sensitive product was isolated by dissolving the flux with degassed DMF under inert atmosphere and then washing with anhydrous ether to give red needle-like crystals, water soluble flux, and elemental Se. This product was allowed to stir in a solution of triethylphosphine (PEt_3) (0.1 mL)/ether (20 mL) for 2 h. Washing with ether gave red crystals of $K_2FeP_2Se_6$ but also black $Fe_2P_2Se_6$ as a minor impurity phase (~5−10%). The presence of $Fe_2P_2Se_6$ was detected by X-ray powder diffraction. Several attempts to obtain pure $K_2FeP_2Se_6$ failed. Semiquantitative microprobe analysis on the red single crystals gave $K_{1.8}Fe_{1.0}P_{1.8}Se_{4.9}$ (average of three data acquisitions). These crystals were used for crystallographic studies. Pure sample for magnetic susceptibility measurements was obtained by manual separation of $K_2FeP_2Se_6$ crystals. Far-IR (CsI matrix) gave absorbances at 475 (s), 466 (s), and 303 (m) cm^{-1}. Direct combination reactions with Fe/P/K_2Se/Se at 500 °C gave similar results.

$Cs_2FeP_2Se_6$ (V). A 0.014 g (0.25 mmol) sample of Fe, 0.343 g (0.75 mmol) of P_2Se_5, 0.172 g (0.50 mmol) of Cs_2Se, and 0.197 g (2.50 mmol) of Se were heated as in the procedure for **IV**. The product was

(9) (a) Pfeiff, R.; Kniep, R. *J. Alloys Compd.* **1992**, *186*, 111−133. (b) Evain, M.; Boucher, F.; Brec, R.; Mathey, Y. *J. Solid State Chem.* **1991**, *90*, 8−16. (c) Lee, S.; Colombet, P.; Ouvrard, G.; Brec, R. *Mater. Res. Bull.* **1986**, *21*, 917−928. (d) Leblanc, A.; Ouili, Z.; Colombet, P. *Mater. Res. Bull.* **1985**, *20*, 947−954.
(10) Lacroix, P. G.; Clement, R.; Nakatani, K.; Zyss, J.; Ledoux, I. *Science* **1994**, *263*, 658−660.
(11) Garin, J.; Parthe, E. *Acta Crystallogr.* **1972**, *B28*, 3672−3674.
(12) Fritz, I. J.; Isaacs, T. J.; Gottlieb, M.; Morosin, B. *Solid State Commun.* **1978**, *27*, 535.
(13) (a) O'Neal, S. C.; Pennington, W. T.; Kolis, J. W. *Angew. Chem., Int. Ed. Engl.* **1990**, *29*, 1486−1488. (b) Zhao, J.; Pennington, W. T.; Kolis, J. W. *J. Chem. Soc., Chem. Commun.* **1992**, 265−266.
(14) Feher, F. In *Handbuch der Praparativen Anorganischen Chemie*; Brauer, G., Ed.; Ferdinand Enke: Stuttgart, Germany, 1954; pp 280−281.
(15) McCarthy, T. J.; Ngeyi, S.-P.; Liao, J.-H.; DeGroot, D.; Hogan, T.; Kannewurf, C. R.; Kanatzidis, M. G. *Chem. Mater.* **1993**, *5*, 331−340.

(16) Abbreviations: s = strong; m = medium; w = weak; v = very.

isolated as in the procedure for **IV** above to give 0.112 g of red needle-like crystals (52% yield, based on Fe). Semiquantitative microprobe analysis on single crystals gave $Cs_{1.9}Fe_{1.0}P_{1.6}Se_{5.6}$ (average of three data acquisitions). Far-IR (CsI matrix) shows absorptions at 478 (s) and 469 (m) cm^{-1}.

$Cs_2Cu_2P_2Se_6$ (VI). A 0.016 g (0.25 mmol) sample of Cu, 0.228 g (0.5 mmol) of P_2Se_5, 0.172 g (0.5 mmol) of Cs_2Se, and 0.197 g (2.5 mmol) of Se were heated as in the procedure for **IV**. The product was isolated by dissolving the flux with degassed DMF under inert atmosphere and then washed with anhydrous ether to give dark green rectangular block-like crystals and some water soluble flux. The residual flux was removed by washing the product with distilled water, MeOH, and ether to give 0.061 g (53% yield based on Cu) of dark green crystals. Semiquantitative microprobe analysis on single crystals gave $Cs_{1.3}Cu_{1.3}P_{1.0}Se_{3.2}$ (average of three data acquisitions). Far-IR (CsI matrix) gave absorptions at 467 (m), 454 (s), 447 (msh), 302 (m), and 213 (vw) cm^{-1}.

$K_2Ag_2P_2Se_6$ (VII). A 0.027 g (0.25 mmol) sample of Ag, 0.228 g (0.5 mmol) of P_2Se_5, 0.079 g (0.5 mmol) of K_2Se, and 0.197 g (2.5 mmol) of Se were heated as in the procedure for **IV**. The product was isolated with DMF and washed with ether. Further washing with 0.1 mL of PEt_3 in ether (20 mL) gave 0.052 g (50% yield, based on Ag) of orange crystals. Semiquantitative microprobe analysis on single crystals gave $K_{1.0}Ag_{1.1}P_{1.0}Se_{2.9}$ (average of three data acquisitions). Far-IR (CsI matrix) gave absorbances at 460 (m), 443 (s), and 302 (w) cm^{-1}. The proper formula of this compound based on the unit cell contents is $K_3Ag_3P_3Se_9$; however, for the sake of simplicity and uniformity with its other analogs (**VI** and **VIII**), we refer to it in this paper as $K_2Ag_2P_2Se_6$.

$Cs_2Ag_2P_2Se_6$ (VIII). A 0.027 g (0.25 mmol) sample of Ag, 0.228 g (0.5 mmol) of P_2Se_5, 0.172 g (0.5 mmol) of Cs_2Se, and 0.197 g (2.5 mmol) of Se were heated as in the procedure for **IV**. The product was isolated with DMF and washed with ether. Further washing with 0.1 mL $P(Et)_3$ in ether (20 mL) gave 0.084 g (66% yield, based on Ag) of yellow-orange needle-like crystals. Semiquantitative microprobe analysis on single crystals gave $Cs_{1.0}Ag_{1.3}P_{1.1}Se_{3.2}$ (average of three data acquisitions). Far-IR (CsI matrix) shows absorptions at 452 (w, br) and 302 (w) cm^{-1}.

2.3. Physical Measurements. FT-IR spectra were recorded as solids in a CsI matrix. The samples were ground with dry CsI into a fine powder, and pressed into translucent pellets. The spectra were recorded in the far-IR region (600−100 cm^{-1}, 4 cm^{-1} resolution) with the use of a Nicolet 740 FT-IR spectrometer equipped with a TGS/PE detector and silicon beam splitter.

Semiquantitative microprobe analyses of the compounds were performed with a JEOL JSM-35C scanning electron microscope (SEM) equipped with a Tracor Northern Energy Dispersive Spectroscopy (EDS) detector. Data acquisition was performed with an accelerating voltage of 20 kV and a 1 min accumulation time.

Optical diffuse reflectance measurements were made at room temperature with a Shimadzu UV-3101PC double beam, double-monochromator spectrophotometer operating in the 200−2500 nm region. The instrument was equipped with an integrating sphere and controlled by a personal computer. The measurement of diffuse reflectance can be used to obtain values for the band gap which agree rather well with values obtained by absorption measurements from single crystals of the same material. The digitized spectra were processed using the Kaleidagraph software program. $BaSO_4$ powder was used as reference (100% reflectance). The data were processed as described earlier.[15]

Differential thermal analysis (DTA) was performed with a computer-controlled Shimadzu DTA-50 thermal analyzer. The ground single crystals (~15.0 mg total mass) were sealed in quartz ampoules under vacuum. An empty quartz ampoule of equal mass was sealed and placed on the reference side of the detector. The samples were heated to the desired temperature at 10 °C/min, and kept there for 10 min followed by cooling at 10 °C/min to 100 °C and finally by rapid cooling to room temperature. Indium (reported mp 156.6 °C) and antimony (reported mp 630.9 °C) served as calibration standards. The reported DTA temperatures are peak temperatures. The DTA samples were examined by powder X-ray diffraction after the experiments.

Magnetic susceptibility measurements were carried out using a MPMS Quantum Design SQUID magnetometer over the range 2−300 K. Single crystals were ground to a fine powder to minimize possible anisotropic effects. In the case of $K_2FeP_2Se_6$, single crystals were carefully hand-picked from the product mixture because of the presence of the minor $Fe_2P_2Se_6$ impurity phase. Corrections for the diamagnetism of the PVC sample containers were applied. Field dependence measurements were performed (at 5 and 300 K) to determine if the samples experienced saturation of their magnetic signal. For all compounds, magnetization increased linearly with increasing field over the range investigated (0−10 000 G). A suitable magnetic field was chosen from the linear region for temperature dependence measurements (2000−3000 G). The μ_{eff} and Θ values were calculated by least-squares fits for the plots of $1/\chi_M$ vs temperature in the paramagnetic (Curie−Weiss) region from 30 to 300 K.

2.4. Crystallographic Studies. All compounds were examined by X-ray powder diffraction (XRD) for the purpose of phase purity and identification. Accurate d_{hkl} spacings (Å) were obtained from the powder patterns recorded on a Rigaku rotating anode (Cu Kα) X-ray powder diffractometer, Rigaku-Denki/RW400F2 (Rotaflex), at 45 kV and 100 mA with a 1°/min scan rate.

Single crystal X-ray diffraction data were collected on a Rigaku AFC6 diffractometer and the $\omega/2\theta$ scan technique was used. None of the crystals showed any significant intensity decay as judged by three check reflections measured every 150 reflections throughout the data collections. Unique data sets were collected in all cases. The space groups were determined from systematic absences and intensity statistics. The structures were solved by direct methods of SHELXS-86[17] and refined by full-matrix least-squares techniques of the TEXSAN package of crystallographic programs.[18] An empirical absorption correction based on ψ-scans was applied to each data set, followed by a DIFABS[19] correction to the isotropically refined structure. The range of transmission factors following the ψ correction were as follows: 0.445−1.000 for **I**, 0.397−1.000 for **III**, 0.447−1.000 for **IV**, 0.473−1.000 for **VII**, and 0.621−1.000 for **VIII**. An extinction correction was made to all the data. All atoms were eventually refined anisotropically. All calculations were performed on a VAXstation 3100/76 computer.

In the case of $Cs_2Cu_2P_2Se_6$, inspection of the residual electron density map revealed two peaks of 2.3 and 2.7 $e^-/Å^3$ that were ~1.4 Å away from Cu(1) and Cu(2). These sites are located near the centers of symmetry in between the Cu···Cu pairs. Refinement of these pseudooctahedral sites as Cu positions resulted in no change in R/R_w and in less than 5% occupancy. The presence of these small peaks were judged statistically insignificant based on the reflection data at hand. However, the complete absense of some Cu^{2+} centers from the lattice cannot be enterely ruled out, particularly in view of the green appearance of these crystals. No residual electron density peaks were found near the Ag atoms in $Cs_2Ag_2P_2Se_6$.

The complete data collection parameters and details of the structure solution and refinement for **I**, **III**, **IV**, **VI**, **VII**, and **VIII** are given in Table 1. The coordinates of all atoms, average temperature factors, and their estimated standard deviations are given in Tables 2−7.

3. Results and Discussion

3.1. Synthesis, Spectroscopy, and Thermal Analysis. The syntheses were a result of a redox reaction in which the metal is oxidized by polyselenide ions in the $A_x[P_ySe_z]$ flux. The metal cation centers are then coordinated by the highly charged $[P_2Se_6]^{4-}$ ligands. The molten *polyselenophosphate* flux method is very effective for crystal growth in this system and quite conducive for isolation of pure products. Triethylphosphine has been shown to be very useful for the removal of insoluble byproducts such as $A_x[P_ySe_z]$ species and elemental Se.

(17) Sheldrick, G. M. In *Crystallographic Computing 3*; Sheldrick, G. M., Kruger, C., Doddard, R., Eds.; Oxford University Press: Oxford, England, 1985; pp 175−189.
(18) TEXSAN: Single Crystal Structure Analysis Software, Version 5.0 (1981). Molecular Structure Corportion, The Woodlands, TX 77381.
(19) Walker, N.; Stuart, D. *Acta Crystallogr.* **1983**, *A39*, 158−166.

Table 1. Crystallographic Data for **I**, **III**, **IV**, **VI**, **VII**, and **VIII**

	I	III	IV	VI	VII	VIII
formula	$K_2MnP_2Se_6$	$Cs_2MnP_2Se_6$	$K_2FeP_2Se_6$	$Cs_2Cu_2P_2Se_6$	$K_3Ag_3P_3Se_9$[b]	$Cs_2Ag_2P_2Se_6$
fw	668.84	856.46	669.75	928.61	1244.46	1017.25
a, Å	6.5349(9)	6.4761(9)	6.421(2)	9.958(3)	8.528(6)	6.807(3)
b, Å	12.696(3)	13.006(2)	12.720(5)	13.067(3)	11.251(6)	12.517(3)
c, Å	7.589(2)	7.974(1)	7.535(3)	10.730(2)	20.975(4)	8.462(3)
α, deg	90.0	90.0	90.0	90.0	90.0	90.0
β, deg	102.67(2)	93.09(1)	102.58(3)	102.46(2)	93.24(3)	95.75(3)
γ, deg	90.0	90.0	90.0	90.0	90.0	90.0
Z; V, Å^3	2; 614.3(4)	2; 670.6(2)	2; 600.7(7)	4; 1363(1)	4; 2009(3)	2; 717.3(8)
λ(Mo Kα), Å	0.710 73	0.710 73	0.710 73	0.710 73	0.710 73	0.710 73
space group	$P2_1/n$ (No. 14)	$P2_1/n$ (No. 14)	$P2_1/n$ (No. 14)	$P2_1/c$ (No. 14)	$P2_1/c$ (No. 14)	$P2_1/n$ (No. 14)
crystal dimens, mm	0.08 × 0.12 × 0.20	0.03 × 0.08 × 0.30	0.05 × 0.10 × 0.30	0.10 × 0.20 × 0.40	0.05 × 0.10 × 0.40	0.03 × 0.08 × 0.30
D_{calc}, g/cm^3	3.616	4.239	3.703	4.524	4.114	4.709
μ, cm^{-1}	195.19	225.67	201.59	244.14	198.57	229.30
$2\theta_{max}$, deg	50	50	50	60	50	50
temp, °C	23	23	23	23	23	23
final R/R_w,[a] %	2.9/3.4	2.7/3.1	3.9/4.5	5.6/6.7	4.5/6.4	3.4/3.9
tot. no. of data	1236	1361	1213	4163	4009	1433
tot. no. of unique data (av)	1134	1245	1113	3943	3745	1322
data with $F_o^2 > 3\sigma(F_o^2)$	755	676	683	2029	1866	733
no. of variables	53	53	53	110	164	56

[a] $R = \sum(|F_o| - |F_c|)/\sum|F_o|$. $R_w = \{\sum w(|F_o| - |F_c|)^2/\sum w|F_o|^2\}^{1/2}$. [b] Although $K_3Ag_3P_3Se_9$ is the proper formula of this compound, for the sake of simplicity and uniformity with its other analogs (**VI** and **VIII**), we will refer to it as $K_2Ag_2P_2Se_6$.

Table 2. Fractional Atomic Coordinates and B_{eq} Values for $K_2MnP_2Se_6$ with Estimated Standard Deviations in Parentheses

atom	x	y	z	B_{eq},[a] Å^2
Se(1)	0.2128(1)	0.32791(7)	0.9293(2)	2.79(4)
Se(2)	0.1797(1)	0.58455(8)	0.7431(1)	2.53(4)
Se(3)	−0.3123(1)	0.44005(8)	0.7311(1)	2.60(4)
Mn(1)	1/2	1/2	1.0000	2.07(7)
P(1)	0.0130(3)	0.4666(2)	0.8665(3)	1.49(8)
K(1)	0.2245(3)	0.8097(2)	1.0394(4)	4.0(1)

[a] B values for anisotropically refined atoms are given in the form of the isotropic equivalent displacement parameters defined as $B_{eq} = (4/3)[a^2B(1,1) + b^2B(2,2) + c^2B(3,3) + ab(\cos\gamma)B(1,2) + ac(\cos\beta)B(1,3) + bc(\cos\alpha)B(2,3)$.

Table 3. Fractional Atomic Coordinates and B_{eq} Values for $Cs_2MnP_2Se_6$ with Estimated Standard Deviations in Parentheses

atom	x	y	z	B_{eq},[a] Å^2
Cs	0.2453(1)	0.82963(7)	1.02388(8)	2.79(4)
Se(1)	0.2378(2)	0.3319(1)	0.9664(1)	2.05(5)
Se(2)	0.2283(2)	0.5736(1)	0.7540(1)	1.92(5)
Se(3)	−0.2492(2)	0.4195(1)	0.7536(1)	2.01(5)
Mn	1/2	1/2	1.0000	2.0(1)
P	0.0437(4)	0.4609(2)	0.8816(3)	1.4(1)

[a] B values for anisotropically refined atoms are given in the form of the isotropic equivalent displacement parameters defined as $B_{eq} = (4/3)[a^2B(1,1) + b^2B(2,2) + c^2B(3,3) + ab(\cos\gamma)B(1,2) + ac(\cos\beta)B(1,3) + bc(\cos\alpha)B(2,3)$.

Due to the stability of these phases, direct stoichiometric combination reactions M/P/A_2Se/Se at 500 °C were implemented for the preparation of large quantities of pure material. This was particularly useful in the Mn system. The presence of colored DMF solutions during isolation of the products from these reactions suggests that some excess $A_x[P_ySe_z]$ flux was present resulting from incomplete mixing during these reactions. Direct combination reactions in the Fe system resulted in impure material with the known ternary phase, $Fe_2P_2Se_6$, as the impurity.

The alkali−selenophosphate flux is important in preparing $K_2Cu_2P_2Se_6$ and $K_2Ag_2P_2Se_6$, as pure materials could not be synthesized from stoichiometric reactions.

Varying the flux composition resulted in the formation of different compounds. In the Mn/P_2Se_5/K_2Se/Se system, increasing the Lewis basicity of the flux, by doubling the amount of K_2Se, resulted in the formation of red-orange water-soluble crystals that analyzed for $K_{4.0}Mn_{1.0}P_{2.0}Se_{8.4}$. The solubility and elemental analysis suggest a molecular compound, perhaps $K_4Mn(PSe_4)_2$. Increased amounts of P_2Se_5 resulted in the formation of the known compound $Mn_2P_2Se_6$. In the Fe/P_2Se_5/A_2Se/Se (A = K, Cs) systems, doubling the amount of A_2Se afforded $FeSe_2$. All reactions with Co and Ni resulted in the stable binary pyrites ($CoSe_2$ and $NiSe_2$).

Table 4. Fractional Atomic Coordinates and B_{eq} Values for $K_2FeP_2Se_6$ with Estimated Standard Deviations in Parentheses

atom	x	y	z	B_{eq},[a] Å^2
Se(1)	0.2218(2)	0.3298(1)	0.9321(2)	2.50(6)
Se(2)	0.1876(2)	0.5841(1)	0.7458(2)	2.29(6)
Se(3)	−0.3185(2)	0.4410(1)	0.7334(2)	2.35(6)
Fe	1/2	1/2	1.0000	1.8(1)
P	0.0144(5)	0.4667(2)	0.8667(5)	1.4(1)
K	0.2246(6)	0.8077(3)	1.0432(5)	3.6(2)

[a] B values for anisotropically refined atoms are given in the form of the isotropic equivalent displacement parameters defined as $B_{eq} = (4/3)[a^2B(1,1) + b^2B(2,2) + c^2B(3,3) + ab(\cos\gamma)B(1,2) + ac(\cos\beta)B(1,3) + bc(\cos\alpha)B(2,3)$.

Table 5. Fractional Atomic Coordinates and B_{eq} Values for $Cs_2Cu_2P_2Se_6$ with Estimated Standard Deviations in Parentheses

atom	x	y	z	B_{eq},[a] Å^2
Cs(1)	0.6126(1)	0.3221(1)	0.1187(1)	2.45(5)
Cs(2)	1.1343(1)	0.1549(1)	0.1595(1)	2.69(5)
Se(1)	0.3607(2)	0.1657(1)	−0.1123(2)	2.23(7)
Se(2)	0.8462(2)	0.1767(1)	0.3762(2)	1.88(7)
Se(3)	1.0054(2)	0.4060(1)	0.2603(2)	2.13(7)
Se(4)	0.7775(2)	0.0768(1)	0.0181(2)	1.64(6)
Se(5)	0.7503(2)	0.5739(2)	−0.0142(2)	2.25(8)
Se(6)	0.4961(2)	0.5810(1)	0.2393(2)	2.03(7)
Cu(1)	0.5486(2)	0.4520(2)	0.4040(2)	2.5(1)
Cu(2)	0.0172(3)	0.4002(2)	0.0378(2)	3.0(1)
P(1)	0.2146(4)	0.0403(3)	−0.1671(4)	1.1(1)
P(2)	0.7197(4)	0.4607(3)	−0.1688(4)	1.2(1)

[a] B values for anisotropically refined atoms are given in the form of the isotropic equivalent displacement parameters defined as $B_{eq} = (4/3)[a^2B(1,1) + b^2B(2,2) + c^2B(3,3) + ab(\cos\gamma)B(1,2) + ac(\cos\beta)B(1,3) + bc(\cos\alpha)B(2,3)$.

Table 6. Fractional Atomic Coordinates and B_{eq} Values for $K_2Ag_2P_2Se_6$ with Estimated Standard Deviations in Parentheses

atom	x	y	z	B_{eq},[a] Å^2
Ag(1)	0.5399(3)	0.1570(2)	0.2781(1)	3.3(1)
Ag(2)	0.1814(4)	0.0387(3)	0.3638(1)	4.9(1)
Ag(3)	0.8686(3)	0.2194(2)	0.3972(1)	3.7(1)
Se(1)	0.7647(3)	0.4246(3)	0.4406(1)	2.5(1)
Se(2)	0.8274(3)	0.2472(3)	0.2727(1)	1.9(1)
Se(3)	0.4483(3)	−0.0552(2)	0.3107(1)	1.6(1)
Se(4)	0.5165(3)	0.6416(3)	0.3538(1)	2.3(1)
Se(5)	1.1559(3)	0.1958(3)	0.4522(1)	2.0(1)
Se(6)	1.2695(3)	−0.0106(3)	0.5771(1)	1.9(1)
Se(7)	0.4093(3)	0.3242(3)	0.3541(1)	2.1(1)
Se(8)	0.9135(3)	0.1670(3)	0.5870(1)	2.1(1)
Se(9)	0.9125(3)	0.5601(3)	0.2649(1)	2.1(1)
K(1)	0.1877(7)	0.3442(7)	0.2096(3)	3.0(3)
K(2)	0.5316(7)	0.2078(7)	0.5095(3)	3.4(3)
K(3)	−0.1365(8)	0.0254(7)	0.0999(3)	3.8(3)
P(1)	0.5964(7)	0.4579(6)	0.3600(3)	1.4(3)
P(2)	0.7285(7)	0.4266(6)	0.2700(3)	1.4(3)
P(3)	1.0699(7)	0.0758(7)	0.5256(3)	1.5(3)

[a] B values for anisotropically refined atoms are given in the form of the isotropic equivalent displacement parameters defined as $B_{eq} = (4/3)[a^2B(1,1) + b^2B(2,2) + c^2B(3,3) + ab(\cos\gamma)B(1,2) + ac(\cos\beta)B(1,3) + bc(\cos\alpha)B(2,3)$.

Table 7. Fractional Atomic Coordinates and B_{eq} Values for $Cs_2Ag_2P_2Se_6$ with Estimated Standard Deviations in Parentheses

atom	x	y	z	B_{eq},[a] Å^2
Cs	0.2465(2)	0.33282(9)	0.9891(1)	2.94(5)
Ag	0.0405(2)	0.4404(1)	1.3586(2)	3.59(7)
Se(1)	−0.2213(2)	0.1785(1)	1.0414(2)	2.50(7)
Se(2)	0.2367(2)	0.0923(1)	1.2465(2)	2.56(7)
Se(3)	−0.1806(2)	−0.0830(1)	1.2496(2)	2.05(6)
P	−0.0383(6)	0.0403(3)	1.1141(5)	1.6(2)

[a] B values for anisotropically refined atoms are given in the form of the isotropic equivalent displacement parameters defined as $B_{eq} = (4/3)[a^2B(1,1) + b^2B(2,2) + c^2B(3,3) + ab(\cos\gamma)B(1,2) + ac(\cos\beta)B(1,3) + bc(\cos\alpha)B(2,3)$.

Similar investigations in the $Mn/P_2Se_5/Na_2Se/Se$ system resulted in the formation of a new phase as evidenced by EDS and XRD. This product crystallizes as an air-sensitive, golden-brown, thin platelike material. Attempts to grow crystals suitable for single crystal X-ray analysis are in progress.[20]

The far-IR spectra of $A_2MP_2Se_6$ (M = Mn, Fe), shown in Table 8, display two strong absorptions at ~480 and ~465 cm^{-1}. These vibrations can be assigned to PSe_3 stretching modes by analogy with $Mn_2P_2Se_6$ (444 cm^{-1}).[21] A description of the medium absorption band at ~305 cm^{-1} in $A_2MP_2Se_6$ is not as straightforward. In $Mn_2P_2Se_6$, a medium absorbance at 316 cm^{-1} was ascribed to an out-of-phase PSe_3 mode, corresponding to a P−P vibration. The P−P vibration is expected to be IR inactive because it resides on a center of symmetry, however, it was not observed in the Raman spectrum. Similar results were obtained for $Na_4P_2S_6{\cdot}6H_2O$.[20] The spectra of $Na_4P_2S_6{\cdot}6H_2O$ were described in terms of internal modes of PS_3 groups and combinations of in-phase and out-of-phase translational and rotational motions.[21] By analogy to these compounds, the medium intensity absorption band at ~305 cm^{-1} for $A_2MP_2Se_6$ can tentatively be ascribed to the out-of-phase translational PSe_3 mode. The weak absorptions below 200 cm^{-1} in $A_2MnP_2Se_6$ have been assigned to translational motions of the metal ions.[21] The spectrum of $K_2MnP_2Se_6$ is shown in Figure 1a. The $A_2M'_2P_2Se_6$ (M′ = Cu, Ag) compounds possess absorptions in the 440−470 cm^{-1} range which have been assigned to PSe_3 stretching modes by analogy to the $A_2MP_2Se_6$ compounds. The absorption at 302 cm^{-1} can be assigned to the out-of-phase PSe_3 translational mode (see Table 8). The far-IR spectra of $Cs_2Cu_2P_2Se_6$ and $K_2Ag_2P_2Se_6$ are shown in parts b and c of Figure 1.

The optical absorption properties of **I**−**VIII** were assessed by studying the UV/near-IR reflectance spectra of the materials. The spectra confirm the semiconducting nature of the materials by revealing the presence of abrupt optical gaps. The $A_2MnP_2Se_6$ (A = K, Rb, Cs) compounds exhibit steep absorption edges from which the band-gap, E_g, can be assessed at 2.33 (**I**), 2.41 (**II**), and 2.19 (**III**) eV, respectively (see Figure 2). The band-gaps of $A_2FeP_2Se_6$ can be assessed at 1.72 (**IV**) and 2.02 (**V**) eV, respectively (see Figure 3). The diffuse reflectance spectrum of $Cs_2Cu_2P_2Se_6$ suggests the presence of two band gaps at ~0.8 and 2.44 eV (see Figure 4a). The green appearance of these crystals suggests the presence of divalent copper in the lattice. The band gaps of **VII** and **VIII** are 2.39 and 2.55 eV and are shown in parts b and c of Figure 4. Higher energy absorptions are readily resolved in these spectra and are assigned to electronic Se→M charge transfer transitions. The difference between the band gaps of $K_2Ag_2P_2Se_6$ (2.39 eV) and $Cs_2Ag_2P_2Se_6$ (2.55 eV) can be attributed to the change in the structural architectures of the two compounds. The Ag−Se orbital overlap in the well-separated one-dimensional chains of $Cs_2Ag_2P_2Se_6$ is expected to be lower than that of the three-dimensional $K_2Ag_2P_2Se_6$ compound. This is facilitated by the increased coordination number of Ag in the K^+ compound. This effect gives rise to broader bands and thus a smaller band gap for $K_2Ag_2P_2Se_6$.

Differential thermal analysis (DTA) shows that all compounds melt congruently, suggesting that large single crystals can be grown from the melt. Table 9 shows optical and melting point data for all compounds.

3.2. Description of Structures. $A_2MP_2Se_6$. The structure of the $[MP_2Se_6]_n^{2n-}$ (M = Mn, Fe) anion is closely related to the TiI_3 structure type. Doubling of the TiI_3 formula gives Ti_2I_6. The $[MP_2Se_6]_n^{2n-}$ anion can be viewed as an ordered substitution of two octahedrally coordinated Ti atoms by M and P_2 respectively and a replacement of six iodine atoms by Se. The transition metal ion and the P−P pairs of $K_2MnP_2Se_6$ reside in Se octahedra that share triangular faces in the a-direction (Figure 5a). These chains are well separated by alkali metal ions (Figure 5b).

Mn resides on an inversion center with Mn−Se bond distances ranging from 2.737(2) to 2.818(2) Å with a normal P−P′ bond of 2.243(5) Å and P−Se distances ranging from 2.173(3) to 2.183(3) Å. The Mn−Mn′ distance is 6.5249(9) Å. Inspection of the Se(1)−Mn−Se(2) angle of 78.38(3)° for $K_2MnP_2Se_6$ reveals a deviation from an ideal octahedral geometry. This small angle is due to a strained four-membered (Mn−Se(1)−P−Se(2)) ring whereas the less strained five-membered envelope-shaped rings give rise to Se(1)−Mn−Se(3) and Se(2)−Mn−Se(3) angles of 88.23(3) and 88.60(3)°, respectively. Se(1) and Se(2) are above (1.809 Å) and below (−1.730 Å) the calculated Mn−Se(3)−P−P′ least-squares plane.

There are small differences between the crystal structures of $Cs_2MnP_2Se_6$ and $K_2MnP_2Se_6$ as evidenced by unit cell β angles of 93.09(1) and 102.67(2)°, respectively. In addition, there is a reduction of the a-axis upon moving from K to Cs which corresponds to a shortening of the Mn−Mn distance from 6.5249(9) to 6.476(2) Å. A slight reorientation of the $[P_2Se_6]^{4-}$ ligand results in a Mn−Se(3)−P angle of 99.07(7)° in $K_2MnP_2Se_6$ and 95.82(8)° in the Cs analog. This conformational change is probably due to differences in packing forces caused by the

(20) McCarthy, T. J.; Chondroudis, K.; Kanatzidis, M. G. Work in progress.
(21) Mathey, Y.; Clement, R.; Sourisseau, C.; Lucazeau, G. *Inorg. Chem.* **1980**, *19*, 2773−2779.

Table 8. Far-IR Data (cm^{-1}) for $A_2MP_2Se_6$ and $A_2M'_2P_2Se_6$ Compounds

$K_2MnP_2Se_6$	$Rb_2MnP_2Se_6$	$Cs_2MnP_2Se_6$	$K_2FeP_2Se_6$	$Cs_2FeP_2Se_6$	$Cs_2Cu_2P_2Se_6$	$K_2Ag_2P_2Se_6$	$Cs_2Ag_2P_2Se_6$
478 (s)	480 (s)	481 (s)	475 (s)	478 (s)	467 (m)	460 (m)	452 (w, br)
463 (s)	465 (s)	464 (s)	466 (s)	469 (m)	454 (s)		
303 (m)	304 (m)	305 (m)	303 (m)		447 (msh)	443 (s)	
210–143 (w)	201–148 (w)	189–152 (w)			302 (m)	302 (w)	302 (w)
					213 (vw)		

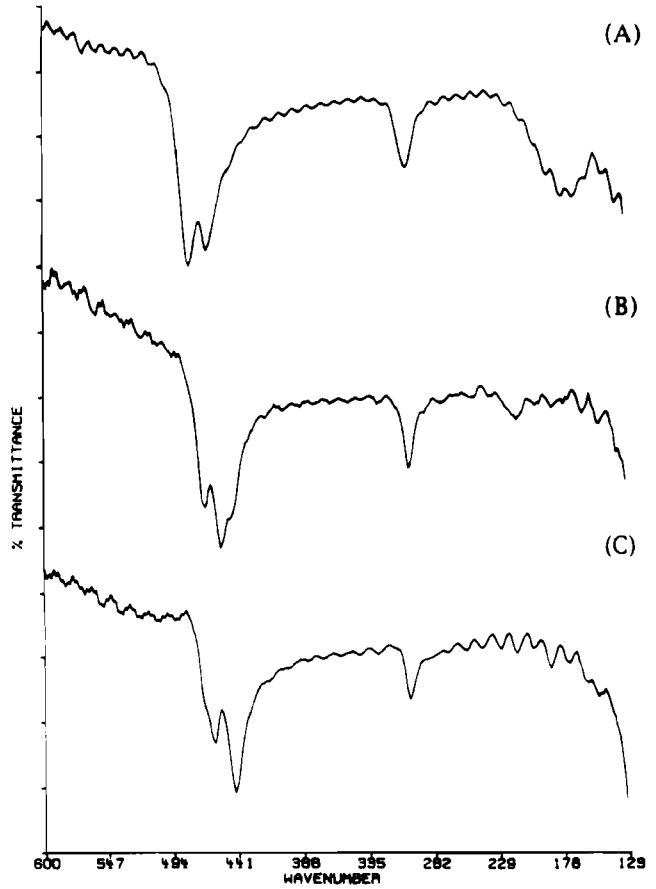

Figure 1. Far-IR spectra of (A) $K_2MnP_2Se_6$, (B) $Cs_2Cu_2P_2Se_6$, and (C) $K_2Ag_2P_2Se_6$.

size difference of the alkali ions. Selected bond distances and angles for **I**, **III**, and **IV** are given in Table 10.

Comparison of $A_2MP_2Se_6$ with the known layered $M_2P_2Q_6$ structure type reveals some interesting structural relationships. It is useful to view the MP_2Se_6 chains deriving from the $M_2P_2Se_6$ lattice as a consequence of the substitution of one M^{2+} by two K^+ cations. A single layer of $M_2P_2Q_6$ is shown in Figure 6a. The M atoms form a hexagonal network and the $[P_2Q_6]^{4-}$ ligand coordinates to three different metal centers as shown in structure **A**.

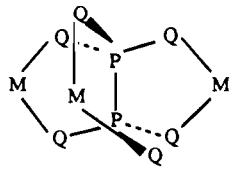

A

Removal of half of the M^{2+} cations gives the $[MP_2Q_6]^{2-}$ anion as shown in Figure 6b. In order to maintain electroneutrality, two alkali metal ions must be introduced. Although this metal-deficient structure (related to that of $AlCl_3$) may very well be stable with the proper counterion, apparently, the lack of a low energy packing arrangement for the alkali metal atoms

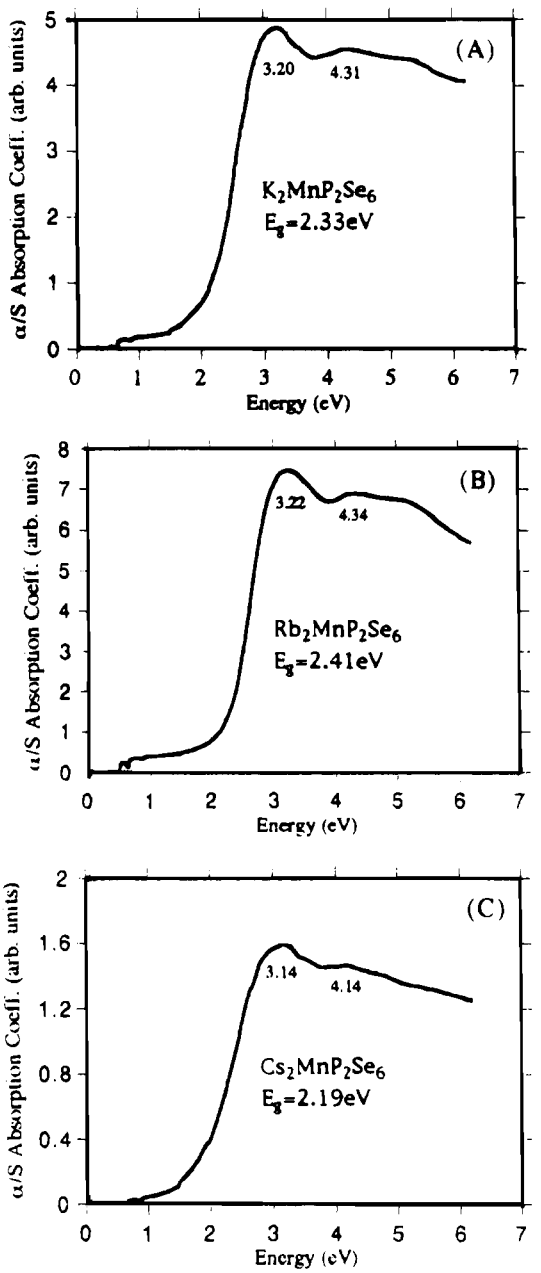

Figure 2. Optical absorption spectra of **I**–**III**.

within the layer causes a structural change to a 1-D structure. This generates more space for efficient packing of the alkali ions. It is interesting to speculate that with alkaline earth cations, such as Ba^{2+}, it may be possible to stabilize the $[MP_2Q_6]^{2-}$ layer.

$Cs_2Cu_2P_2Se_6$. The structure of the $[Cu_2P_2Se_6]_n^{2n-}$ anion is closely related to the $A_2MP_2Se_6$ structure type and is shown in Figure 7a. The M^{2+} ions are replaced by weakly interacting $Cu^+\cdots Cu^+$ dimers that alternate with the P–P pairs along the [101] direction.

The Cu(1)···Cu(1′) and Cu(2)···Cu(2′) distances are 2.761(5) and 2.731(5) Å respectively. For comparison, the Cu–Cu distance in copper metal is 2.56 Å. This attractive interaction

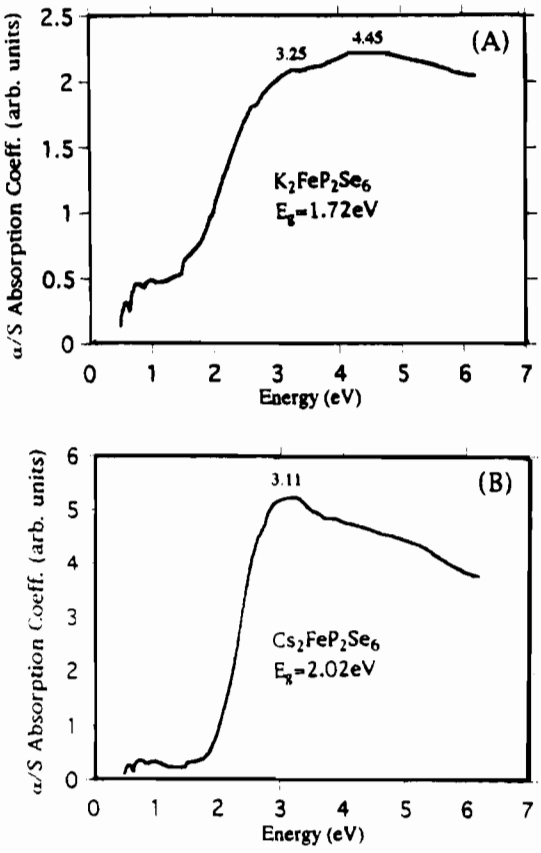

Figure 3. Optical absorption spectra of **IV** and **V**.

also leads to the displacement of Cu(1) and Cu(2) from their respective trigonal planes by 0.2 Å. These "classical" $d^{10}-d^{10}$ interactions have been observed in both molecular[22] or solid state structures such as KCu_3S_2,[23] $K_3Cu_8S_6$,[24] $Cs_3Cu_8Se_6$,[25] and KCuS.[26] Theoretical calculations have shown that mixing of empty 4s and 4p orbitals with occupied 3d orbitals in these dimers lowers the energy of the σ and σ^* orbitals.[27] It has also been proposed for several $d^{10}-d^{10}$ complexes that the bridging ligands force the metals closer in order to maximize M−L interactions.[28] Since $Cs_2Cu_2P_2Se_6$ features two $[P_2Se_6]^{4-}$ bridging ligands for each dimer, it is possible that the multidentate $[P_2Se_6]^{4-}$ coordination is playing an important role in forcing the metals to close proximity. It is not clear whether the interactions contribute significantly in determining the structure or the metals are simply forced to tolerate the short contact due to packing forces. It is probable that the $A_2MP_2Se_6$ structure type is quite stable, and since Cu^+ does not prefer an octahedral coordination and by itself is not enough to balance the negative charge on that octahedral site, it forms pairs of $CuSe_3$ trigonal planes to conform to the imposed geometry.

The Cu−Se distances range from 2.373(3) to 2.417(4) Å which compare well with values for other Cu−Se trigonal planar centers as in $(Ph_4P)_4[Cu_2(Se_4)(Se_5)_2]$[29] and $(Ph_4P)_2{}^-[Cu_4(Se_4)_{2.4}(Se_5)_{0.6}]$.[30] The Se(1)−Cu(1)−Se(6) and Se(3)−Cu(2)−Se(5) angles are less than 120° at 110.6(1)° because of strained (Cu−Se−P−P′−Se) five-membered rings whereas the remaining Se−Cu−Se angles range from 121.3(1) to 125.7(1)°. The shortest Cu−Se distances for Cu(1) (2.373(3) Å) and Cu(2) (2.375(3) Å) are trans to the small 110.6(1)° angle as more space is allowed for Se(2) and Se(4) to get closer to the metal center.

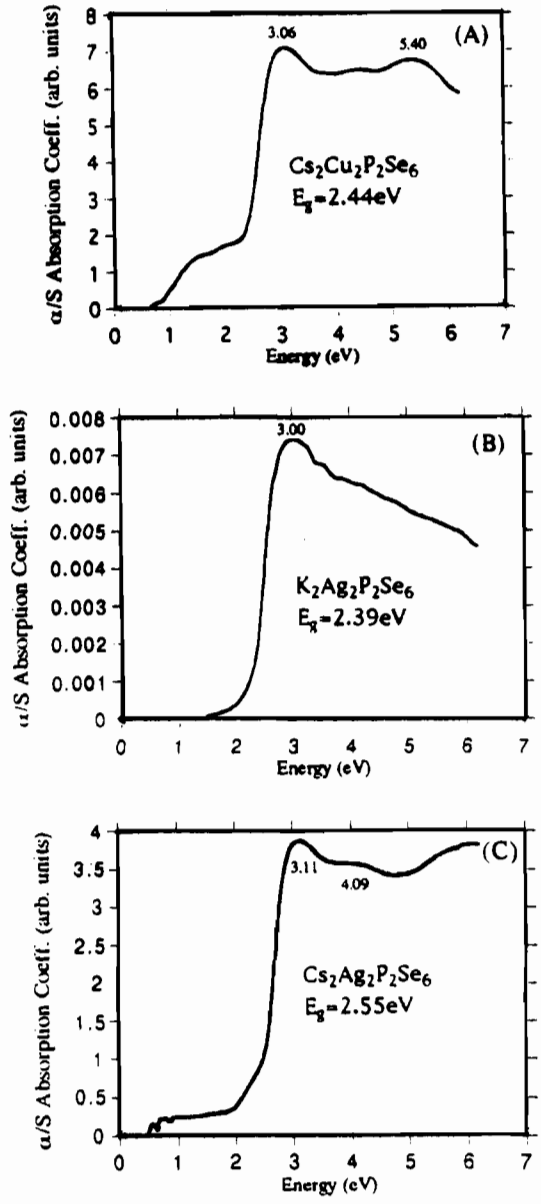

Figure 4. Optical absorption spectra of **VI**−**VIII**.

Table 9. Optical Band Gaps and Melting Point Data for $A_2MP_2Se_6$ and $A_2M'_2P_2Se_6$

formula	E_g, eV	mp, °C
$K_2MnP_2Se_6$	2.33	717
$Rb_2MnP_2Se_6$	2.41	781
$Cs_2MnP_2Se_6$	2.19	831
$K_2FeP_2Se_6$	1.72	662
$Cs_2FeP_2Se_6$	2.02	769
$Cs_2Cu_2P_2Se_6$	2.44	670
$K_2Ag_2P_2Se_6$	2.39	542
$Cs_2Ag_2P_2Se_6$	2.55	594

(22) (a) Dance, I. G. *Polyhedron* **1983**, *2*, 1031−1043. (b) Hollander, F. J.; Coucouvanis, D. *J. Am. Chem. Soc.* **1977**, *99*, 6268−6279. (c) Chadha, R.; Kumar, R.; Tuck, D. G. *J. Chem. Soc., Chem. Commun.* **1986**, 188−189. (d) Coucouvanis, D.; Murphy, C. N.; Kanodia, S K. *Inorg. Chem.* **1980**, *19*, 2993−2998.
(23) Burschka, C.; Bronger, W. *Z. Naturforsch.* **1977**, *32B*, 11−14.
(24) Burschka, C. *Z. Naturforsch.* **1979**, *34B*, 675−677.
(25) Schils, H.; Bronger, W. *Z Anorg. Allg. Chem.* **1979**, *456*, 187−193.
(26) Savelberg, G.; Schäfer, H. *Z. Naturforsch.* **1978**, *33B*, 711−713.
(27) (a) Merz, K. M.; Hoffmann R. *Inorg. Chem.* **1988**, *27*, 2120−2127. (b) Mehrotra, P. K.; Hoffmann, R. *Inorg. Chem.* **1978**, *17*, 2187−2189.
(28) (a) Cotton, F. A.; Feng, X.; Matusz, M.; Poli, R. *J. Am. Chem. Soc.* **1988**, *110*, 7077−7083. (b) Lee, S. W.; Trogler, W. C. *Inorg. Chem.* **1990**, *29*, 1659−1662.
(29) Müller, U.; Ha-Eierdanz, M.-L.; Kräuter, G.; Dehnicke, K. *Z. Naturforsch.* **1990**, *45B*, 1128−1132.
(30) Cusick, J.; Scudder, M. L.; Craig, D. C.; Dance, I. G. *Polyhedron* **1989**, *8*, 1139−1141.

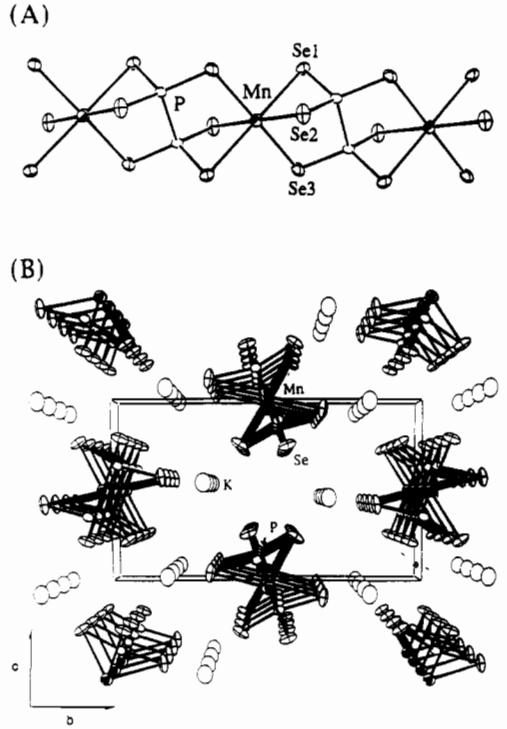

Figure 5. (A) ORTEP representation of a single $[MnP_2Se_6]_n^{2n-}$ chain. (B) Packing diagram of $K_2MnP_2Se_6$ viewed down the [100] direction with labeling.

Selected bond distances and angles for $Cs_2Cu_2P_2Se_6$ are given in Table 11.

$Cs_2Ag_2P_2Se_6$. The structure of the $[Ag_2P_2Se_6]_n^{2n-}$ anion is closely related to that of $Cs_2Cu_2P_2Se_6$and is shown in Figure 7b. The major difference is that the volume is roughly half that of $Cs_2Cu_2P_2Se_6$ so there is only one $Ag^+\cdots Ag^+$ dimer per unit cell. The Ag···Ag distance of 2.919(3) Å falls in the 2.75–3.00 Å range for many solid state Ag compounds with close $Ag^+\cdots Ag^+$contacts.[31] The Ag^+ ions are not displaced from their distorted trigonal planes as is the case for Cu in **VIII**.

The coordination geometry of Ag is distorted trigonal planar with Ag–Se distances ranging from 2.545(2) to 2.641(3) Å. These distances compare well with other Ag–Se trigonal planar species.[32] The Se(1)–Ag–Se(2) angle is less than 120° at 105.55(7)° because of a strained (Ag–Se–P–P′–Se) five-membered envelope-shaped ring whereas the remaining Se–Ag–Se angles are 121.77(8) and 132.04(9)°. The Se(1)–Ag–Se(3) angle of 132.04(9)° is quite large and compares to the 138.8° angle found in the $[(Ph_4P)Ag(Se_4)]_n$ one-dimensional polymer.[32a] The shortest Ag–Se distance (Ag–Se(3) = 2.545(2) Å) is trans to the small 105.55(7)° angle as more space is allowed for the Se(3) to get closer to the metal center. Selected bond distances and angles for $Cs_2Ag_2P_2Se_6$ are given in Table 12.

The existence of $Cu^+\cdots Cu^+$or $Ag^+\cdots Ag^+$ dimers located in octahedral sites in these compounds can hopefully shed some light on the question concerning the nature of Cu(Ag) coordination sites in several cation substitution compounds such as $CuCrP_2S_6$,[33] $CuVP_2S_6$,[5d] $Cu_{0.52}Mn_{1.74}P_2S_6$,[34] and $Ag_2MnP_2S_6$.[9b]

Table 10. Selected Distances (Å) and Angles (deg) for **I**, **III**, and **IV** with Standard Deviations in Parentheses[a]

	$K_2MnP_2Se_6$	$Cs_2MnP_2Se_6$	$K_2FeP_2Se_6$
	Distances		
M–M′	6.5349(9)	6.476(2)	6.421(2)
M–Se(1)	2.853(1)	2.774(1)	2.782(2)
M–Se(2)	2.746(1)	2.737(2)	2.676(2)
M–Se(3)	2.711(1)	2.818(2)	2.614(2)
M–Se(av)	2.77(7)	2.78(4)	2.69(8)
P–P′	2.236(5)	2.243(5)	2.225(7)
P–Se(1)	2.181(2)	2.183(3)	2.182(4)
P–Se(2)	2.181(2)	2.178(3)	2.176(3)
P–Se(3)	2.176(2)	2.173(3)	2.180(4)
P–Se(av)	2.179(3)	2.178(5)	2.179(3)
A–Se(1)	3.677(4)	3.916(2)	3.683(5)
A–Se(1′)	3.399(3)	3.773(2)	3.398(4)
A–Se(1″)		3.950(2)	
A–Se(2)	3.607(3)	3.965(2)	3.597(4)
A–Se(2′)	3.322(3)	3.880(2)	3.330(4)
A–Se(2″)		3.757(2)	
A–Se(3)	3.433(3)	3.978(2)	3.414(4)
A–Se(3′)	3.525(3)	3.742(2)	3.538(4)
A–Se(3″)	3.602(3)	3.695(2)	3.573(4)
A–Se(av)	3.5(1)	3.9(1)	3.5(1)
	Angles		
Se(1)–M–Se(2)	78.38(3)	80.80(4)	80.11(5)
Se(2)–M–Se(3)	88.60(3)	89.83(5)	87.43(5)
Se(1)–M–Se(3)	88.22(3)	89.30(4)	89.36(5)
M–Se(1)–P	76.15(6)	76.25(8)	75.9(1)
M–Se(2)–P	78.55(6)	77.14(7)	78.4(1)
M–Se(3)–P	99.07(7)	95.82(8)	99.1(1)
Se(1)–P–Se(2)	108.45(9)	110.0(1)	107.4(1)
Se(1)–P–Se(3)	117.0(1)	115.3(1)	118.3(2)
Se(2)–P–Se(3)	115.6(1)	115.8(1)	116.7(2)
Se(1)–P–P′	105.6(1)	104.8(2)	105.4(2)

[a] The estimated standard deviations in the mean bond lengths and the mean bond angles are calculated by the equation $\sigma_l = \{\sum_n (l_n - l)^2/n(n-1)\}^{1/2}$, where l_n is the length (or angle) of the nth bond, l the mean length (or angle), and n the number of bonds.

These compounds adopt the stable $M_2P_2S_6$ structure with cation substitution occurring in the octahedral sites. The crystal structure of $CuCrP_2S_6$reveals a Cu electron density cloud which exhibits three extrema.[33] One of them is in the middle on a pseudo-octahedral site and the other two are near the trigonal sulfur planes which suggests that CuS_6octahedral sites, Cu···Cu pairs, and vacancies all exist at room temperature and can be fit by a disorder model. Complimentary EXAFS[35] studies have confirmed this disorder model, but recent low-temperature neutron powder diffraction studies have disputed the existence of bimetallic entities.[36] $Cu^+\cdots Cu^+$ pairs were also assumed to exist in $CuVP_2S_6$,[5d]which features the same Cu positions as found in $CuCrP_2S_6$plus a third tetrahedral site located in the van der Waals gap. The location of copper atoms in $Cu_{0.52}Mn_{1.74}P_2S_6$ remains uncertain due to some inconsistencies between X-ray diffraction and EXAFS data.[34] It appears that the occurrence of copper pairs in these copper substitution phases is still an open question. In the case of Ag, the structure determination of $Ag_2MnP_2S_6$[9b]confirmed the presence of two silver atoms per octahedron with 81% of the Ag(1) atoms found in trigonal planar coordination (Ag–Ag = 3.38 Å). On each side of Ag(1) are two sites of minor contribution (Ag(2) 13%; Ag(3) 8%). We think that the unequivocal presence of $M^+\cdots M^+$ pairs in our compounds serves to support the presence

(31) Janzen, M. *Angew. Chem. Int. Ed. Engl.* **1987**, *26*, 1098–1110.
(32) (a) Huang, S.-P.; Kanatzidis, M. G. *Inorg. Chem.* **1991**, *30*, 1455–1466. (b) Kanatzidis, M. G.; Huang, S.-P. *J. Am. Chem. Soc.* **1989**, *111*, 760–761.
(33) Colombet, P.; Leblanc, A; Danot, M.; Rouxel, J. *J Solid State Chem.* **1982**, *41*, 174–184.
(34) Maisonneuve, V.; Cajipe, V. B.; Payen, C. *Chem. Mater.* **1993**, *5*, 758–760.
(35) Mathey, Y.; Michalowicz, A.; Toffoli, P.; Vlaic, G. *Inorg. Chem.* **1984**, *23*, 897–902.
(36) Mathey, Y.; Mercier, H.; Michalowicz, A.; Leblanc, A. *J. Phys. Chem. Solids*, **1985**, *46*, 1025–1029.

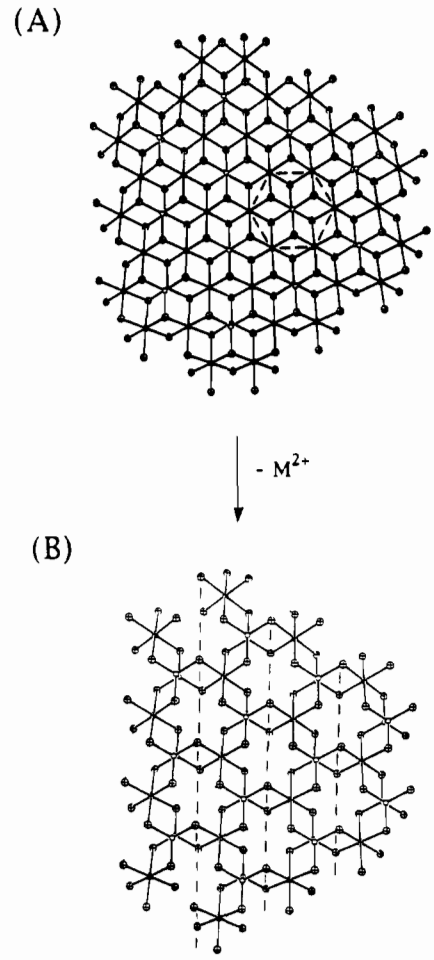

Figure 6. (A) Single $Mn_2P_2Q_6$ layer. The dashed lines indicate the hexagonal arrangement of Mn^{2+} ions. (B) Removal of half of the Mn^{2+} ions resulting in a single layer of the hypothetical $[MnP_2Q_6]_n^{2n-}$ anion. Dashed lines highlight the possibility of chain formation by breaking the corresponding Mn–Se bonds.

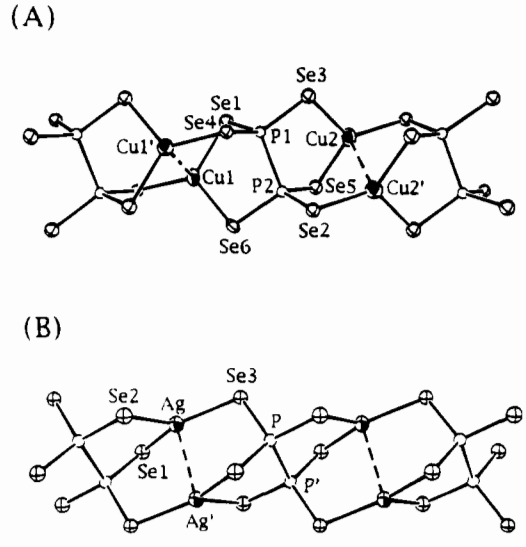

Figure 7. (A) Single $[Cu_2P_2Se_6]_n^{2n-}$ chain. (B) Single $[Ag_2P_2Se_6]_n^{2n-}$ chain.

of $M^+\cdots M^+$pairs in octahedral sites within the layers of $CuM^{III}P_2S_6$ compounds.

$K_2Ag_2P_2Se_6$. The substitution of K for Cs resulted in a dramatic change in the structure of the $[Ag_2P_2Se_6]^{2-}$ anion. $K_2Ag_2P_2Se_6$ possesses a unique but complicated three-dimensional tunnel framework made up of $AgSe_4$ tetrahedra linked by P_2Se_6 units (see Figure 8). The channels run along the crystallographic *a*-axis and are filled with K^+ ions.

There are two types of $[P_2Se_6]^{4-}$ ligands in this structure, see Chart 1. Both ligands contain four Se atoms that each bond to a Ag atom and two Se atoms that each bridge two of these Ag atoms. The P–P bond in type 2 lies on a center of symmetry while that of type 1 does not. In type 2, the two Se atoms that bridge Ag atoms are located on opposite sides of the P–P bond. In type 1, the two Se atoms are situated on the same side of the P–P bond.

These are new bonding modes for the $[P_2Se_6]^{4-}$ ligand and differ from those found in KMP_2Se_6[2] and $Cs_8M_4(P_2Se_6)_5$.[3] The $[P_2Se_6]^{4-}$ units connect $AgSe_4$ tetrahedra as shown in Figure 9.

Table 11. Selected Distances (Å) and Angles (deg) for $Cs_2Cu_2P_2Se_6$ with Standard Deviations in Parentheses[a]

Cu(1)–Cu(1′)	2.761(5)	Se(1)–Cu(1)–Se(4)	125.7(1)
Cu(2)–Cu(2′)	2.731(5)	Se(1)–Cu(1)–Se(6)	110.6(1)
		Se(4)–Cu(1)–Se(6)	121.3(1)
Cu(1)–Se(1)	2.400(3)	Se(2)–Cu(2)–Se(3)	123.7(1)
Cu(1)–Se(4)	2.373(3)	Se(2)–Cu(2)–Se(5)	122.5(1)
Cu(1)–Se(6)	2.416(3)	Se(3)–Cu(2)–Se(5)	110.6(1)
Cu(2)–Se(2)	2.375(3)	Se(1)–Cu(1)–Cu(1′)	87.3(1)
Cu(2)–Se(3)	2.417(4)	Se(5)–Cu(2)–Cu(2′)	84.0(1)
Cu(2)–Se(5)	2.407(4)		
Cu–Se(av)	2.40(2)	Se(1)–P(1)–Se(3)	112.6(2)
		Se(1)–P(1)–Se(4)	114.1(2)
P(1)–P(2)	2.260(6)	Se(3)–P(1)–Se(4)	111.4(2)
		Se(2)–P(2)–Se(5)	114.1(2)
P(1)–Se(1)	2.186(4)	Se(2)–P(2)–Se(6)	110.4(2)
P(1)–Se(3)	2.177(4)	Se(5)–P(2)–Se(6)	113.3(3)
P(1)–Se(4)	2.202(5)	Se–P–Se(av)	113(2)
P(2)–Se(2)	2.186(4)		
P(2)–Se(5)	2.194(5)		
P(2)–Se(6)	2.187(4)		
P–Se(av)	2.189(8)		
Cs(1)–Se(1)	3.733(2)	Cs(2)–Se(1)	3.766(2)
Cs(1)–Se(2)	3.725(2)	Cs(2)–Se(3)	3.766(2)
Cs(1)–Se(2′)	3.847(3)	Cs(2)–Se(3′)	3.711(3)
Cs(1)–Se(4)	3.861(2)	Cs(2)–Se(4)	3.694(2)
Cs(1)–Se(5)	3.948(2)	Cs(2)–Se(4′)	3.780(2)
Cs(1)–Se(5′)	3.797(3)	Cs(2)–Se(5)	3.877(2)
Cs(1)–Se(6)	3.887(2)	Cs(2)–Se(6)	3.733(2)
Cs(1)–Se(6′)	3.759(2)	Cs–Se(av)	3.80(8)
Cs(1)–Se(6″)	3.967(2)		

[a] The estimated standard deviations in the mean bond lengths and the mean bond angles are calculated by the equation $\sigma_l = \{\sum_n(l_n - l)^2/n(n-1)\}^{1/2}$, where l_n is the length (or angle) of the *n*th bond, l the mean length (or angle), and n the number of bonds.

Table 12. Selected Distances (Å) and Angles (deg) for $Cs_2Ag_2P_2Se_6$ with Standard Deviations in Parentheses[a]

Ag–Ag′	2.919(3)	Se(1)–Ag–Se(2)	105.55(7)
		Se(1)–Ag–Se(3)	132.04(9)
Ag–Se(1)	2.595(2)	Se(2)–Ag–Se(3)	121.77(8)
Ag–Se(2)	2.641(3)	Ag–Ag′–Se(2)	94.05(9)
Ag–Se(3)	2.545(2)	Ag–Ag′–Se(3)	95.72(8)
Ag–Se(av)	2.59(5)		
P–Se(1)	2.183(5)	Se(1)–P–Se(2)	110.1(2)
P–Se(2)	2.182(4)	Se(1)–P–Se(3)	115.7(2)
P–Se(3)	2.205(4)	Se(2)–P–Se(3)	109.9(2)
P–Se(av)	2.19(1)	Se(1)–P–P′	106.5(3)
P–P′	2.285(8)		
Cs–Se(1)	3.788(2)	Cs–Se(2″)	3.939(2)
Cs–Se(1′)	3.819(3)	Cs–Se(3)	3.790(2)
Cs–Se(1″)	4.091(3)	Cs–Se(3′)	3.663(3)
Cs–Se(2)	3.720(2)	Cs–Se(3″)	3.725(2)
Cs–Se(2′)	3.963(3)	Cs–Se(av)	3.8(1)

[a] The estimated standard deviations in the mean bond lengths and the mean bond angles are calculated by the equation $\sigma_l = \{\sum_n(l_n - l)^2/n(n-1)\}^{1/2}$, where l_n is the length (or angle) of the *n*th bond, l the mean length (or angle), and n the number of bonds.

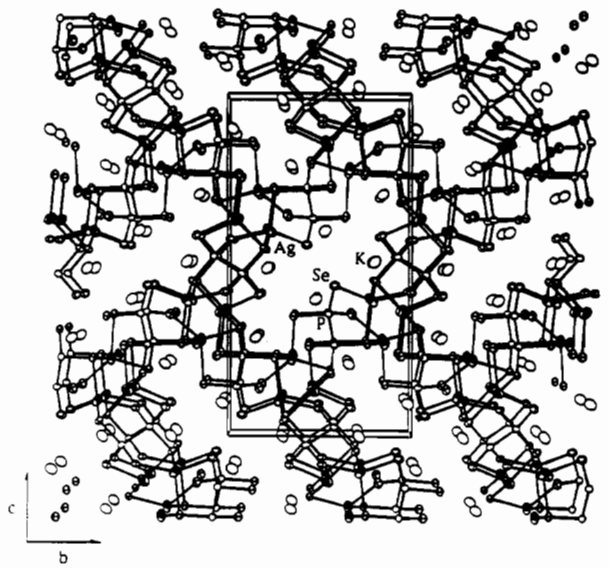

Figure 8. Three-dimensional structure of $K_2Ag_2P_2Se_6$ viewed down the [100] direction with labeling.

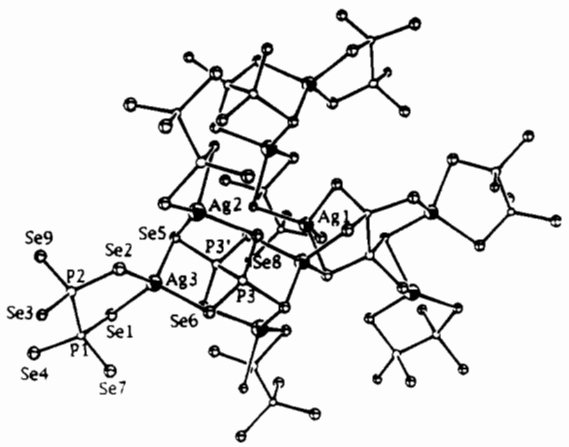

Figure 9. Portion of the $[Ag_2P_2Se_6]_n^{2n-}$ anion showing the complexity of $[P_2Se_6]^{4-}$ binding and the local $AgSe_4$ coordination environment with labeling.

Chart 1

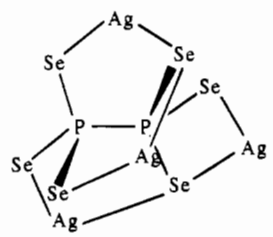

Type 1

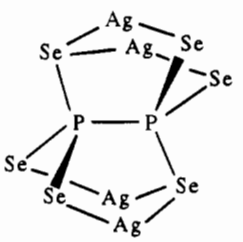

Type 2

For comparison, the $[P_2Se_6]^{4-}$ ligand in the known ternary compound $Ag_4P_2Se_6$ bonds to 10 Ag atoms with two Se atoms each bonding to two Ag atoms and the remaining four Se atoms each bonding to three Ag atoms.[37] In this structure, P_2Se_6 building blocks are assembled into layers and are linked via $AgSe_4$ tetrahedra to form a dense three-dimensional network. As in the case of the one-dimensional $A_2M_2P_2Se_6$ compounds, $K_2Ag_2P_2Se_6$ can also be viewed as a derivative of $Ag_4P_2Se_6$ generated by breaking down the $Ag_4P_2Se_6$ framework by incorporation of $K_4P_2Se_6$. The addition of K_2Se gives rise to a more open channel structure.

(37) Toffoli, P.; Khodadad, P.; Rodier, N. *Acta Crystallogr.* **1978**, *B34*, 1779−1781.

Table 13. Selected Distances (Å) and Angles (deg) for $K_2Ag_2P_2Se_6$ with Standard Deviations in Parentheses[a]

Ag(1)−Ag(2)	3.869(4)	K(1)−Se(4)	3.702(8)
Ag(1)−Ag(3)	3.715(4)	K(1)−Se(6)	3.454(7)
Ag(1)−Se(2)	2.662(4)	K(1)−Se(7)	3.487(7)
Ag(1)−Se(3)	2.615(4)	K(1)−Se(8)	3.379(7)
Ag(1)−Se(4)	2.786(4)	K(1)−Se(9)	3.614(8)
Ag(1)−Se(7)	2.743(4)	K(1)−Se(9′)	3.360(8)
Ag(2)−Se(3)	2.797(4)	K(2)−Se(4)	3.376(7)
Ag(2)−Se(3)	2.578(4)	K(2)−Se(5)	3.361(7)
Ag(2)−Se(3)	2.678(4)	K(2)−Se(6)	3.661(8)
Ag(2)−Se(3)	2.783(4)	K(2)−Se(6′)	3.384(7)
Ag(3)−Se(1)	2.653(4)	K(2)−Se(7)	3.613(8)
Ag(3)−Se(1)	2.633(4)	K(2)−Se(8)	3.586(7)
Ag(3)−Se(1)	2.662(4)	K(3)−Se(4)	3.676(8)
Ag(3)−Se(1)	2.695(4)	K(3)−Se(5)	3.867(9)
Ag−Se(av)	2.69(7)	K(3)−Se(7)	3.423(8)
		K(3)−Se(8)	3.499(9)
P(1)−P(2)	2.278(8)	K(3)−Se(9)	3.351(8)
P(3)−P(3′)	2.31(1)	K−Se(av)	3.5(2)
P(1)−Se(1)	2.188(7)		
P(1)−Se(4)	2.178(8)		
P(1)−Se(7)	2.191(7)		
P(2)−Se(2)	2.186(8)		
P(2)−Se(3)	2.213(7)		
P(2)−Se(9)	2.180(7)		
P(3)−Se(5)	2.205(7)		
P(3)−Se(6)	2.192(7)		
P(3)−Se(8)	2.165(7)		
P−Se(av)	2.19(1)		

Se(2)−Ag(1)−Se(3)	130.5(1)	Se(1)−P(1)−Se(4)	113.4(3)
Se(2)−Ag(1)−Se(4)	95.1(1)	Se(1)−P(1)−Se(7)	111.7(3)
Se(3)−Ag(2)−Se(5)	130.4(1)	Se(4)−P(1)−Se(7)	115.0(3)
Se(3)−Ag(2)−Se(9)	80.9(1)	Se(2)−P(2)−Se(3)	110.5(3)
Se(1)−Ag(3)−Se(6)	122.1(1)	Se(2)−P(2)−Se(9)	111.1(3)
Se(1)−Ag(3)−Se(2)	102.0(2)	Se(3)−P(2)−Se(9)	111.1(3)
		Se(5)−P(3)−Se(6)	109.7(3)
		Se(5)−P(3)−Se(8)	111.5(3)
		Se(6)−P(3)−Se(8)	113.9(3)

[a] The estimated standard deviations in the mean bond lengths and the mean bond angles are calculated by the equation $\sigma_l = \{\sum_n (l_n - l)^2/n(n-1)\}^{1/2}$, where l_n is the length (or angle) of the nth bond, l the mean length (or angle), and n the number of bonds.

Selected distances and angles for $K_2Ag_2P_2Se_6$ are found in Table 13. Ag(1,2) are located in distorted tetrahedral coordination environments as evidenced by Se−Ag−Se angles that range from 95.1(1) to 130.5(1)° for Ag(1) and from 80.9(1) to 130.4(1)° for Ag(2). Ag(3) resides in a fairly regular tetrahedral site with normal angles (103.2(1)−122.1(1)°). The Ag(1,2,3)−Se bond distances fall in the 2.578(4)−to 2.797(4) Å range which compares well with the values observed in $Ag_4P_2Se_6$.[37] No Ag···Ag contacts are observed as the Ag−Ag distances are long at 3.715(4) and 3.869(4) Å. Normal P−P bonds in the $[P_2Se_6]^{4-}$ ligands are observed at 2.278(8) and 2.31(1) Å and the P−Se bonds are typical for Se atoms in bridging positions (2.19(1) Å (mean)).

The higher coordination number of Ag^+ most likely results from the effect the relatively small K^+ cation exerts on the $[Ag_2P_2Se_6]^{2-}$ structure. A correlation between the metal coordination number (CN) and the size of the counterion was observed and discussed in the Ag^+/Se_x^{2-} system earlier.[32a] The change of the CN for Ag^+ from three, in $Cs_2Ag_2P_2Se_6$, to four, in $K_2Ag_2P_2Se_6$, agrees with the general trend identified in group 10 polychalcogenides that larger counterions favor a small CN for the group 10 metal. While a high CN will produce compact structures, a small CN tends to result in expanded or low dimensional structures.

3.3. Magnetic Susceptibility. The temperature dependent magnetic susceptibility was collected for $K_2MnP_2Se_6$ (**I**), Rb_2-

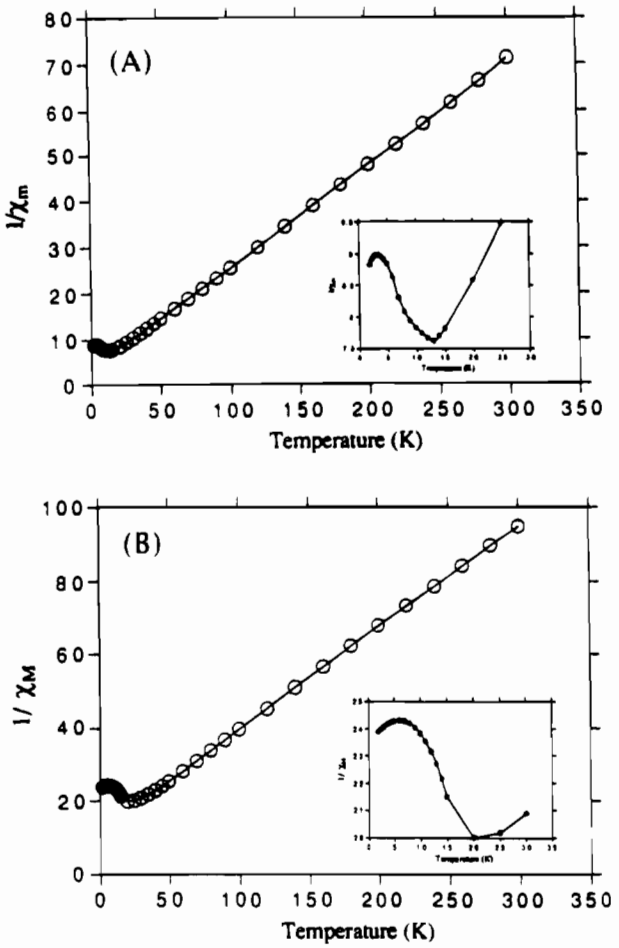

Figure 10. Plots of $1/\chi_M$ vs T taken at 2000 G of applied field in the temperature range of 2−300 K for (A) $Cs_2Mn_2P_2Se_6$ and (B) $K_2FeP_2Se_6$. The inset graphs show expanded views of the region 2−30 K.

Table 14. Magnetic Parameters for **I**−**IV**

formula	μ_{eff}, μ_B	Θ, K	T_N, K
$K_2MnP_2Se_6$	5.8	−25	10
$Rb_2MnP_2Se_6$	5.6	−18	12
$Cs_2MnP_2Se_6$	6.0	−14	13
$K_2FeP_2Se_6$	5.4	−43	20

MnP_2Se_6 (**II**), $Cs_2MnP_2Se_6$ (**III**), and $K_2FeP_2Se_6$ (**IV**). All compounds are paramagnetic above ~30 K and obey Curie−Weiss law. Typical susceptibility plots at 2000 G are shown in Figure 10 for **III** and **IV**. Table 14 lists the magnetic parameters for **I**−**IV**. The calculated moments are 5.8, 5.6, 6.0, and 5.4 μ_B for **I**−**IV**, respectively. These values indicate that the M^{2+} ions in these compounds are in high-spin configurations and agree well with the calculated spin-only moments ($\mu_{eff} = [4S(S+1)]^{1/2}$). For comparison, the magnetic moments for $Mn_2P_2Se_6$ and $Fe_2P_2Se_6$ are 6.1 and 5.1 μ_B, respectively.[38] Below 30 K, the susceptibility show maxima indicating antiferromagnetic coupling below this temperature. Since it is well-known that exchange interactions are very sensitive to small changes in the bond length and angles of the bridging system,[39] we hoped to observe such effects in the $A_2MnP_2Se_6$ family of compounds. The effect of the small reduction in the M···M distance and slight reorientation of the $[P_2Se_6]^{4-}$ ligand upon moving from $K_2MnP_2Se_6$ (Mn−Mn = 6.5349(9) Å) to $Cs_2MnP_2Se_6$ (Mn−Mn = 6.476(2) Å) is not reflected in the magnetic data. The Neél temperatures (T_N) for $A_2MnP_2Se_6$ vary between 10 and 13 K with Weiss constants (Θ) in the −14 to −25 K range. Since the M−M distances are large (> 6.4 Å), it is assumed that the weak antiferromagnetic interactions proceed via a superexchange pathway through the bridging $[P_2Se_6]^{4-}$ ligand. A stronger antiferromagnetic interaction is observed in $K_2FeP_2Se_6$ with higher T_N and Θ values of 20 K and −43 K. A similar increase in the interaction upon moving from Mn to Fe is also observed for the strongly antiferromagnetic, two-dimensional $M_2P_2Q_6$ (M = Mn, Fe, Ni) compounds.[38]

Concluding Remarks

The general family of one-dimensional $A_2M(P_2Se_6)$ compounds derives from the well known two-dimensional $M_2P_2Se_6$ family by incorporation of $A_4P_2Se_6$. The synthesis of new quaternary selenophosphates in molten $A_x[P_ySe_z]$ salts provides a useful and broad synthetic methodology that can be applied to main group elements as well as transition metals. The $A_x[P_ySe_z]$ fluxes provide reliably $[P_2Se_6]^{4-}$ units that display remarkable versatility in terms of ligand binding to metals. The high negative charge of these units makes them hard to stabilize in conventional aqueous or organic solvents. It would be interesting to see whether changes in the nominal stoichiometry of these fluxes can result in other $[P_xSe_y]^{n-}$ units as well. For example, by increasing the basicity of the flux, the $[PSe_4]^{3-}$ ligand can be stabilized in $CsPbPSe_4$.[40]

Acknowledgment. Financial support from the National Science Foundation DMR 92-02428, is gratefully acknowledged. The X-ray instrumentation used in this work was purchased in part with funds from the National Science Foundation (CHE-89-08088). This work made use of the SEM facilities of the Center for Electron Optics at Michigan State University.

Supplementary Material Available: Tables of calculated and observed powder diffraction patterns, atomic coordinates of all atoms and anisotropic and isotropic thermal parameters of all non-hydrogen atoms, bond distances and angles, and crystallographic data (33 pages). Ordering information is given on any current masthead page.

IC940971D

(38) (a) Brec, R.; Schleich, D. M.; Ouvrard, G.; Louisy, A.; Rouxel, J. *Inorg. Chem.* **1979**, *18*, 1814−1818. (b) Odile, J.-P.; Steger, J. J.; Wold, A. *Inorg. Chem.* **1975**, *14*, 2400−2402. (c) Taylor, B. E.; Steger, J. J.; Wold, A.; Kostiner, E. *Inorg. Chem.* **1974**, *13*, 2719−2421. (d) Taylor, B. E.; Steger. J. J.; Wold, A. *J. Solid State Chem.* **1973**, *7*, 461−467.
(39) Crawford, V. H.; Richardson, H. W.; Wasson, J. R.; Hodgson, D. J.; Hatfield, W. E., *Inorg. Chem.* **1976**, *15*, 2107−2110.
(40) McCarthy, T. J.; Chondroudis, K.; Kanatzidis, M. G. To be submitted for publication.